JOURNAL OF MATERIALS SCIENCE 22 (1987) 27–36

On the nucleation of θ' and T_1 on Al_3Zr precipitates in Al–Li–Cu–Zr alloys

J. M. GALBRAITH, M. H. TOSTEN, P. R. HOWELL
Department of Materials Science and Engineering, The Pennsylvania State University, University Park, Pennsylvania 16802, USA

Two quaternary Al–Li–Cu–Zr alloys have been investigated using electron microscopy. Ageing at 190° C resulted in the nucleation of θ' precipitates on the Al_3Zr/matrix interface in addition to heterogeneous nucleation on matrix dislocations. In the majority of cases, the broad, coherent face of the θ' plates was in contact with the Al_3Zr precipitates. Similar evidence showed that nucleation of T_1 precipitates occurred on the Al_3Zr, but to a lesser extent than θ'. Solid–solid nucleation theory has been used to account for the Al_3Zr acting as a nucleation substrate.

1. Introduction

The aluminium–lithium system has been the subject of a considerable amount of research [1, 2] because of its obvious applications to aerospace structures. The addition of lithium to aluminium results in a substantial reduction of density and an increase in elastic modulus when compared with conventional aluminium alloys. The current trend in alloy development is directed towards the development of Al–Li–Cu and Al–Li–Cu–Mg alloys because strength levels can approach that of 7075-T651, but with both lower density and higher modulus [3].

Precipitation in the Al–Li–Cu system has been studied extensively and is believed to occur as follows [1, 2]

α-supersaturated solid solution $\rightarrow$ GP zones $\rightarrow$ θ'' $\rightarrow$ θ' $\rightarrow$ θ (Al_2Cu)

$\rightarrow$ δ' (Al_3Li) $\rightarrow$ δ (AlLi)

$\rightarrow$ T_1 (Al_2CuLi)

Excluding the ternary T_1 phase, the decomposition process is similar to those that occur in Al–Li and Al–Cu binary alloys. There is some debate as to the existence of the ternary T_1' metastable phase and the T_B equilibrium phase; their possible existence is still under investigation.

It has been reported that small additions of zirconium to high strength aluminium alloys retards recrystallization and controls grain growth, as well as improves toughness, stress corrosion resistance and quench sensitivity [4, 5]. The principle purpose of adding zirconium to Al–Li–Cu alloys is to form metastable cubic Al_3Zr precipitates which can effectively pin grain and subgrain boundaries. Cubic Al_3Zr (from now on referred to as β') has a $L1_2$ structure with $a = 0.408$ nm. In Al–Zr subperitectic alloys (less than 0.18 wt % Zr), β' is spherical, nucleating heterogeneously on dislocations and boundaries [4]. Depending on the temperature of the pre-age heat treatment for Al–Li–Zr alloys, β' has been found to be semi-coherent or coherent with the matrix. At pre-ageing temperatures above 500° C, β' forms semi-coherently, while coherent β' forms at temperatures below 500° C [6].

Several investigators have shown that δ' precipitates on the β'/matrix interface resulting in a spherical shell of δ' around the β' precipitates [6–9]. The purpose of this paper is to show that β' also serves as a nucleation substrate for θ' and T_1.

It is well established that interphase boundary precipitation is an important process in solid–solid nucleation kinetics. It occurs during the bainite reaction in ferrous [10] and non-ferrous [11] systems and during the formation of a sequence of precipitate phases in alloys undergoing ageing reactions [12]. Heterogeneous nucleation was originally treated by Gibbs [13] for liquids and more recently examined for solids both in the presence and in the absence of facets [14]. It is suggested that the critical nucleus in a solid–solid transformation is likely to be faceted whenever there exists reasonable similarity between the lattices of the precipitate and the matrix. Lattice matching at the facets has been studied in some detail for the special case of precipitate nucleation at a matrix/GP zone boundary [15]. This phenomenon has been observed in a number of aluminium alloys including Al–Zn, Al–Cu, Al–Zn–Mg, and Al–Mg–Si [16–24].

2. Experimental details

The alloys used in this investigation were supplied by the Alloy Technology Division, Alcoa Center, PA and had the following compositions (wt %)

Al–1.0% Li–4.5% Cu–0.12% Zr

Al–2.0% Li–3.0% Cu–0.12% Zr

After hot rolling, specimen material was solution treated at 550° C for 30 min, cold water quenched, deformed 2% in tension and aged at 190° C. Ageing times of 16 and 128 h were employed for the 1.0%

0022–2461/87 $03.00 + .12

TABLE I Phases encountered in the Al–Li–Cu–Zr system at 190° C*

Phase	Composition	Crystal structure	Orientation relationship
δ'*	Al_3Li	$L1_2$	cube–cube
T_2	Al_6CuLi_3	icosahedral	unknown
θ'	Al_2Cu	tetragonal	$(0\,0\,1)_{\theta'} \parallel (0\,0\,1)_\alpha$; $[1\,0\,0]_{\theta'} \parallel [1\,0\,0]_\alpha$
β'	Al_3Zr	$L1_2$	cube–cube
T_1	Al_2CuLi	hexagonal	$(0\,0\,0\,1)_{T_1} \parallel (1\,1\,1)_\alpha$; $[1\,0\,\bar{1}\,0]_{T_1} \parallel [1\,\bar{1}\,0]_\alpha$
T_B	$Al_{75}Cu_4Li$	cubic	$(0\,0\,1)_{T_B} \parallel (0\,0\,1)_\alpha$; $[1\,1\,0]_{T_B} \parallel [1\,0\,0]_\alpha$

*δ' is not observed in the 1.0% Li–4.5% Cu alloy.

Li–4.5% Cu alloy. Times ranging from 0.5 to 520 h were used for the 2.0% Li–3.0% Cu alloy.

Thin foil specimens for transmission electron microscopy (TEM) were prepared in a twin-jet electropolishing unit using 25% nitric acid in methanol. The solution was cooled to −20° C, and an applied potential of 12 V was used. After perforation, the foils were rinsed in ethanol. All TEM was performed using a Philips EM420T operating at 120 kV.

3. Results

Table I lists the compositions, crystal structures and orientation relationships of the precipitate phases found in the alloys investigated. (Note that GP zones and the θ'' phase were not observed.) An inhomogeneous distribution of β' precipitates was present with diameters in the range of 20 to 40 nm. These precipitates had a cube–cube relationship to the matrix and were coherent as shown by the Ashby–Brown strain contrast obtained in the strong two-beam bright field (BF) image of an as quenched 2% Li–3% Cu alloy (Fig. 1). It was possible to determine the misfit between the β' and the matrix from this contrast. This misfit ranged from +0.3% to +0.6%. Further confirmation that these spherical, coherent precipitates are β' was obtained from energy dispersive spectrometry (EDS) analysis which indicated the presence of zirconium in the precipitate. Similar evidence has been obtained by Stimson *et al.* [6], Makin and Ralph [7], and Gregson and Flower [8]. In addition, these precipitates were imaged in centred dark field (CDF) using a $1/2(0\,0\,2)\vec{g}$ superlattice reflection. Fig. 2 is a [1 1 0] selected area diffraction pattern (SADP) of a 1.0% Li–4.5% Cu alloy aged for 128 h which clearly shows the presence of superlattice reflections due to the β'. Superlattice reflections in this alloy can only be from β' since the ordered δ' phase is absent.

Fig. 3a is a BF micrograph of a 1.0% Li–4.5% Cu alloy aged for 128 h ([1 1 0] foil orientation). For this

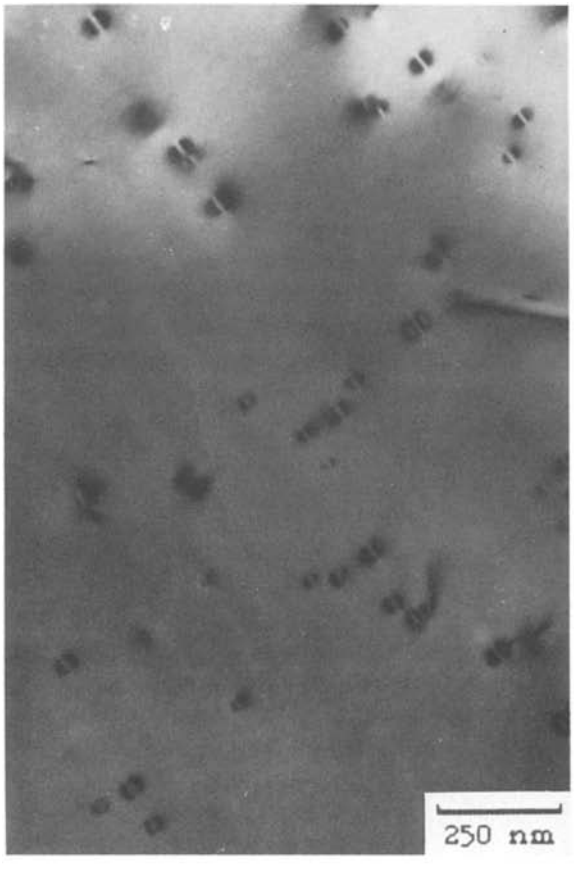

Figure 1 Bright field image of an as quenched 2% Li–3% Cu alloy. The majority of the β' (Al_3Zr) precipitates exhibit Ashby–Brown strain field contrast.

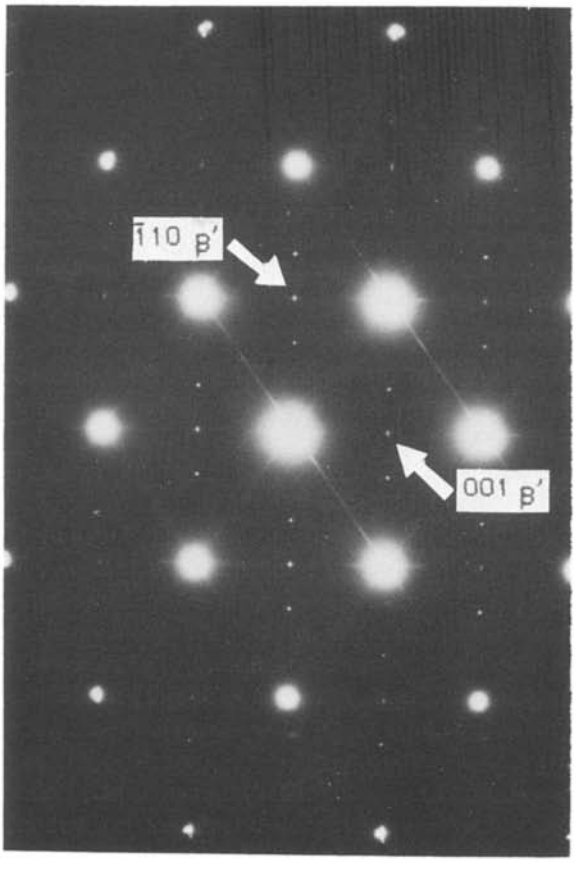

Figure 2 A selected area diffraction pattern ([1 1 0] foil orientation). Note the strong 0 0 1 and $\bar{1}\,1\,0$ β' superlattice reflections (1.0% Li–4.5% Cu alloy aged for 128 h).

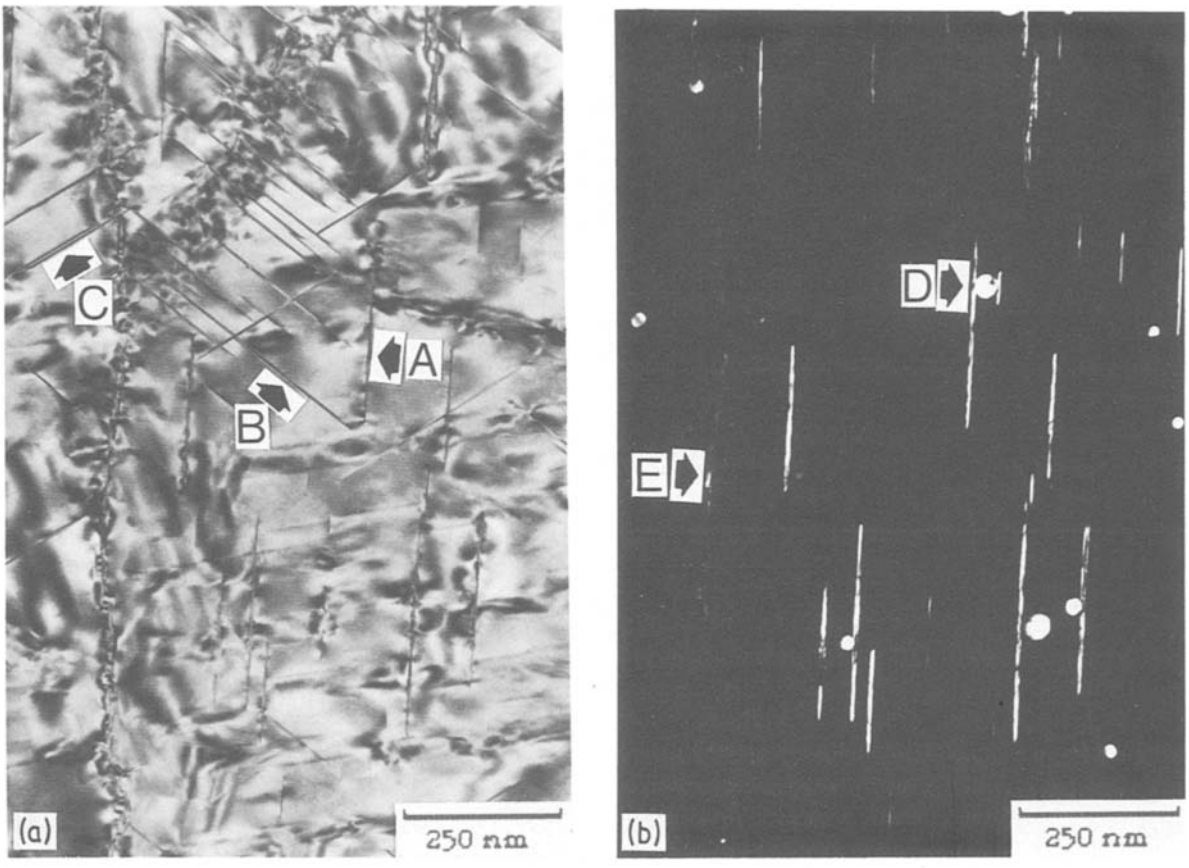

Figure 3 Bright field/dark field pair of the 1.0% Li–4.5% Cu alloy aged for 128 h; (a) bright field image; (b) corresponding β'/θ' dark field image. For discussion, see text.

foil normal, one variant of θ' is upright (arrowed A) and two variants of T_1 are upright (arrowed B and C). Fig. 3b is the CDF corresponding to Fig. 3a. Both β' and the upright θ' variant are imaged since the objective aperture included reflections at $1/2\,(0\,0\,2)\vec{g}$ (due to β') and $2/3\,(0\,0\,2)\vec{g}$ (due to the θ' variant). This CDF micrograph shows several examples of the broad, coherent face of the θ' in contact with the β' (arrowed D). It is also instructive to note the precipitation of θ' on the low angle grain boundary (arrowed E). These θ' plates have smaller diameters than those within the grain. In addition, a higher number density of θ' precipitates is present on the low angle grain boundary. This is a reflection of the high density of lattice dislocations which constitute the boundary. A more detailed discussion of grain boundary precipitation in Al–Li–Cu alloys is presented in Tosten *et al.* [9]. Fig. 4a is another BF micrograph of a 1.0% Li–4.5% Cu alloy aged for 128 h ([1 1 0] foil orientation), and Figs 4b, c and d are corresponding CDF images from the same area. Again, the CDF image formed using the superlattice reflection at $1/2\,(0\,0\,2)\vec{g}$ (Fig. 4b) shows nucleation of θ' on β'. Figs 4c and d illustrate the distribution of the two upright variants of T_1 (CDFS formed using $1/2\,(1\,\bar{1}\,1)\vec{g}$ and $1/2\,(\bar{1}\,1\,1)\vec{g}$ respectively). An interesting observation to note is that two precipitate species are present on the low angle grain boundary (arrowed A in Fig. 4a) as shown in Figs 4b and c. The θ' plates in Fig. 4b and the T_1 plates in Fig. 4c are oriented so that the angle between the habit plane normal and the local boundary normal is relatively small while the T_1 plates in Fig. 4d make an angle of nearly 90°. These observations suggest that the orientation variants of both the θ' and T_1 phases that nucleate on low angle grain boundaries minimize the angle between the local boundary normal and the low energy habit plane normal. This suggestion would explain why T_1 precipitates are absent on the boundary in the lower portion of Fig. 4c where the boundary curves in such a way that the local boundary normal and habit plane normal are at a high angle. Similar observations have been made in other grain boundary precipitation studies [9, 25–27]. It was also found that at least two variants of θ' could nucleate on the same β' precipitate. An example of this is shown in Figs 5a and b ([1 1 2] foil orientation). In the centre of these two figures, a single β' precipitate is associated with two variants of θ'.

The CDF micrograph in Fig. 6 ([1 1 0] foil orientation) is formed using a δ' superlattice reflection in a 2% Li–3% Cu alloy aged for 1.25 h. This figure shows that, in addition to the small spherical δ', δ' is associated with the β', and "plates" of δ' are also observed. However, close examination shows that these "plates" are duplex consisting of an inner, dark imaging core of θ' together with an outer shell of δ'. This trimodal δ' distribution develops in the early stage of ageing and has been noted in a previous study [9]. Of more importance in this investigation is the close association of θ' plates and the two β' precipitates (arrowed A and B). Fig. 7 was recorded from a 2% Li–3% Cu alloy aged for 1.25 h ([0 0 1] foil normal). In this case, two orthogonal sets of duplex θ'/δ' precipitates are imaged (CDF using a δ' superlattice

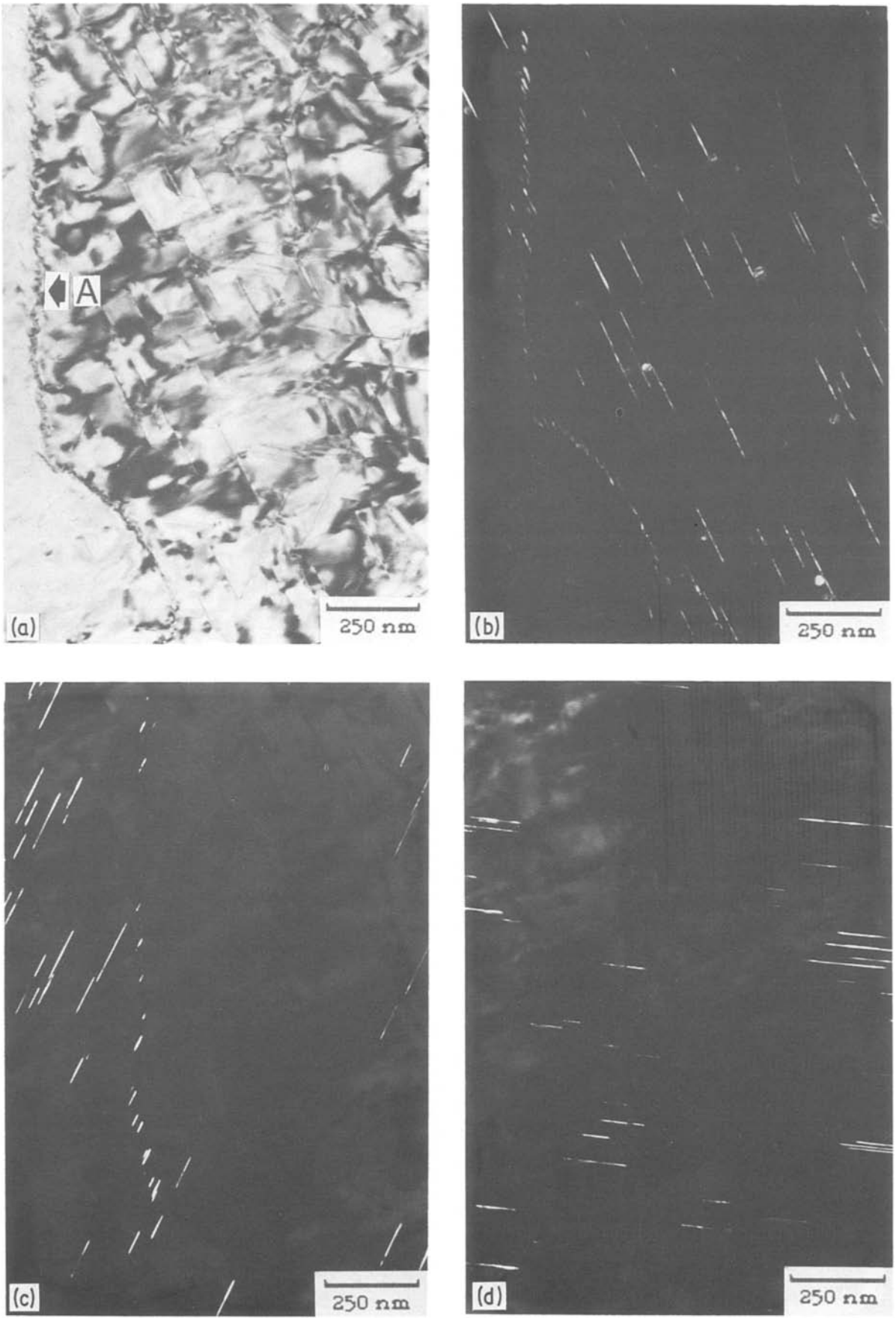

Figure 4 The distribution of the β', θ' and T_1 phases in the 1.0% Li–4.5% Cu alloy aged for 128 h; (a) bright field image; (b) corresponding β'/θ' dark field image; (c) a corresponding T_1 dark field micrograph; (d) a further T_1 dark field image of the area shown in (a).

reflection). The point of interest is that the θ' plates associated with the β' (arrowed A and B) have grown in only one direction from their point of contact, unlike the situation in Fig. 6 where the θ' grew in both directions from the point of contact. It is postulated that growth in the other direction in Fig. 7 is inhibited by the presence of δ' on the β'. This phenomenon also raises the question: can θ' nucleate on δ' which

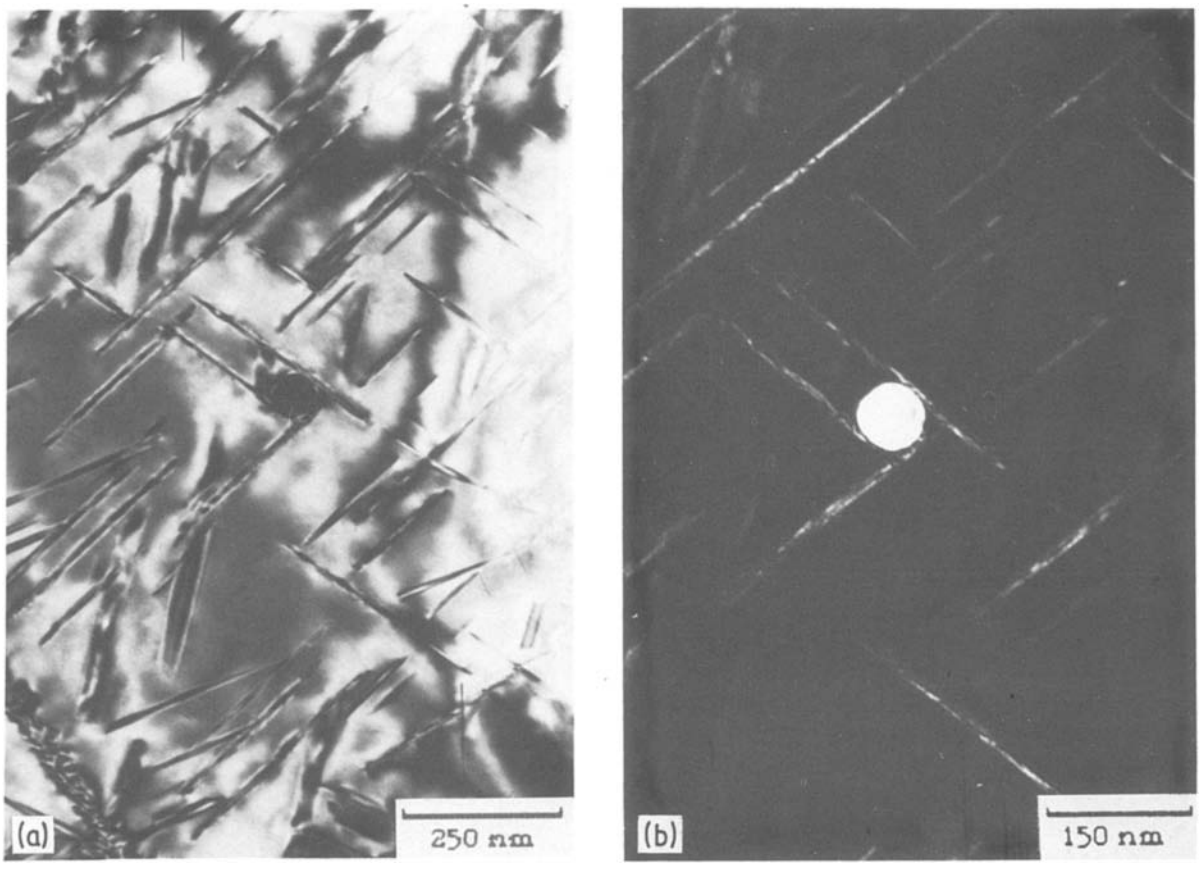

Figure 5 Bright field/dark field pair of the 1.0% Li–4.5% Cu alloy aged for 128 h; (a) bright field image; (b) corresponding β'/θ' dark field image.

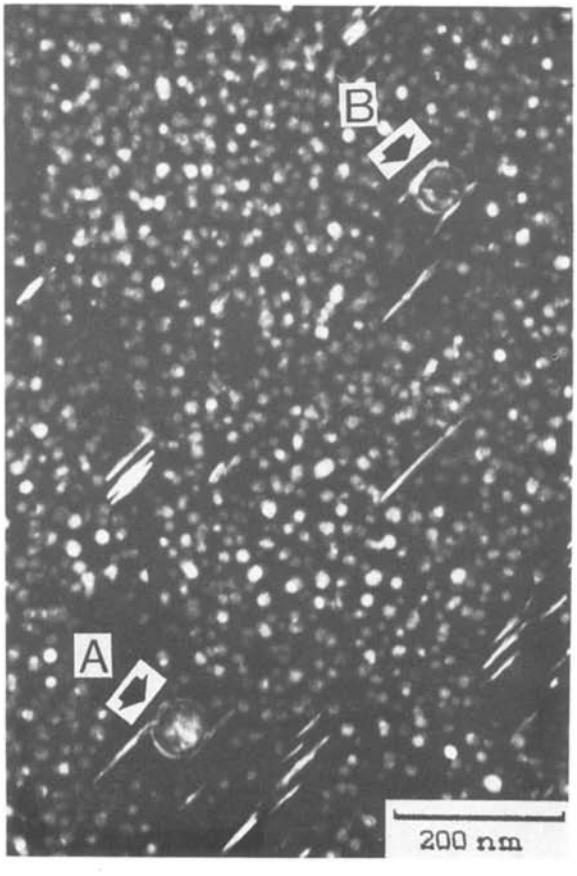

Figure 6 δ' CDF image (2% Li–3% Cu alloy aged for 1.25 h).

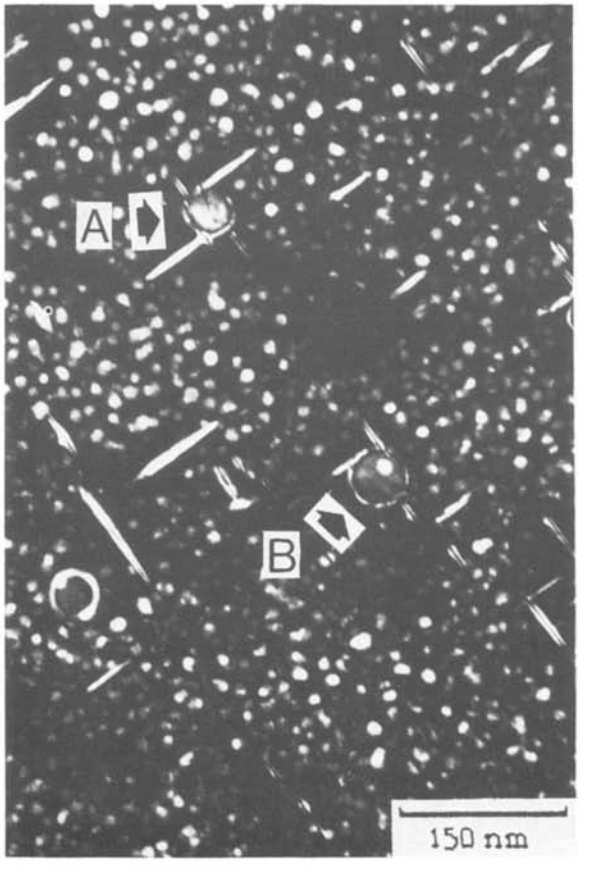

Figure 7 δ' CDF image (2% Li–3% Cu alloy aged for 1.25 h).

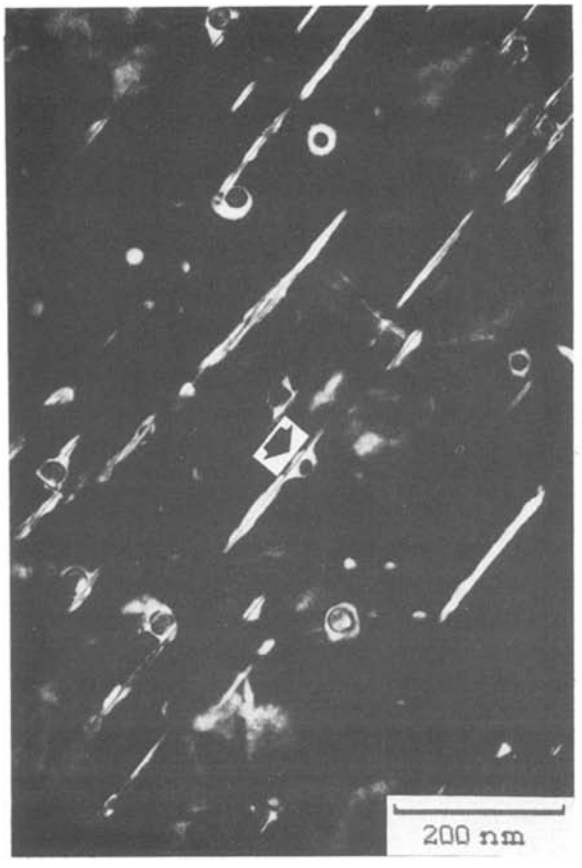

Figure 8 δ' CDF image (2% Li–3% Cu alloy aged for 18 h).

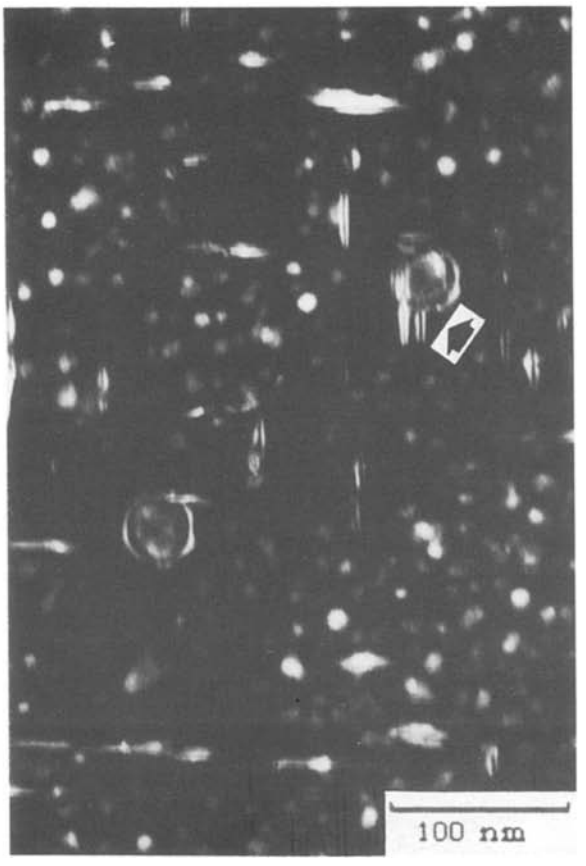

Figure 9 δ' CDF image (2% Li–3% Cu alloy aged for 1.25 h).

commonly encapsulates the β' in this alloy? A possible occurrence of this is shown in Fig. 8 where the dark imaging cores of θ' and β' appear to be separated by a thin coating of δ' (arrowed). However, this was an isolated example and may represent the impingement of a duplex θ'/δ' precipitate with a duplex β'/δ' precipitate. It should also be noted that the β'/δ' interface is not always clearly delineated so that the "thin δ' coating" observed in Fig. 8 may be an imaging artefact. In the vast majority of cases, the θ' appeared to be in direct contact with the β'. Indeed, it is possible that the presence of δ' on the β' could inhibit nucleation of θ' on the β'. This latter contention is substantiated by the lower occurrence of θ' nucleation on β' in the 2% Li–3% Cu alloy (which contains δ') in comparison to the 1.0% Li–4.5% Cu alloy (which does not contain δ').

Although the dominant interaction between θ' and β' involved the broad face of the θ' being in contact with the β', the edge of the θ' plates could also be in contact with the β' as shown in Fig. 9 (arrowed). This type of interaction was observed most frequently in the 2% Li–3% Cu alloy. Further discussion of this phenomenon is presented in Section 4.

Plate-shaped precipitates of T_1 were also found in contact with the β', but the incidence of T_1 nucleation against θ' nucleation on β' was much lower. Fig. 10a is a BF micrograph ([1 1 0] foil orientation) of a 2% Li–3% Cu alloy which had been aged for 30 min; Fig. 10b is the corresponding CDF image using a $1/2(\bar{1}\,1\,1)\vec{g}$ reflection. For this foil normal, two variants of T_1 are upright (although only one variant is shown in these figures). The β' precipitate in the centre of Fig. 10b has two T_1 plates associated with it (arrowed).

Overageing the alloys resulted in the T_1 precipitate becoming the dominant matrix phase at the expense of θ' and, to a lesser extent, δ'. However, both θ' and T_1 were still observed to be in contact with the β'/matrix coherent interface.

4. Discussion

Close examination of a large number of micrographs in both alloys showed that nucleation of the θ' precipitates on the β'/matrix interface occurs frequently. In most cases, the broad, coherent faces of the θ' plates were in contact with the β'. Similar evidence showed the nucleation of T_1 on the β', but to a lesser extent than θ'. Therefore, in the quaternary Al–Li–Cu–Zr alloys, β' acts as a nucleation substrate, not only for δ' as described in previous studies, but also for θ' and T_1. (Similar observations were made in a 2.6% Li–1.0% Cu alloy which had been aged for 16 h.) At this point, it should be emphasized that the results presented in Section 3 cannot be interpreted in terms of impingement events between θ' (or T_1) and β' since:

1. the occurrence of θ' plates in contact with β' is very frequent. For example, in Fig. 4b, virtually every β' precipitate is associated with at least one θ' plate; and
2. in the vast majority of instances (e.g. see Fig. 4b) the broad face of the θ' is in contact with the β'.

The high occurrence of θ' and T_1 nucleation on the β'/matrix interface can be best described in terms of

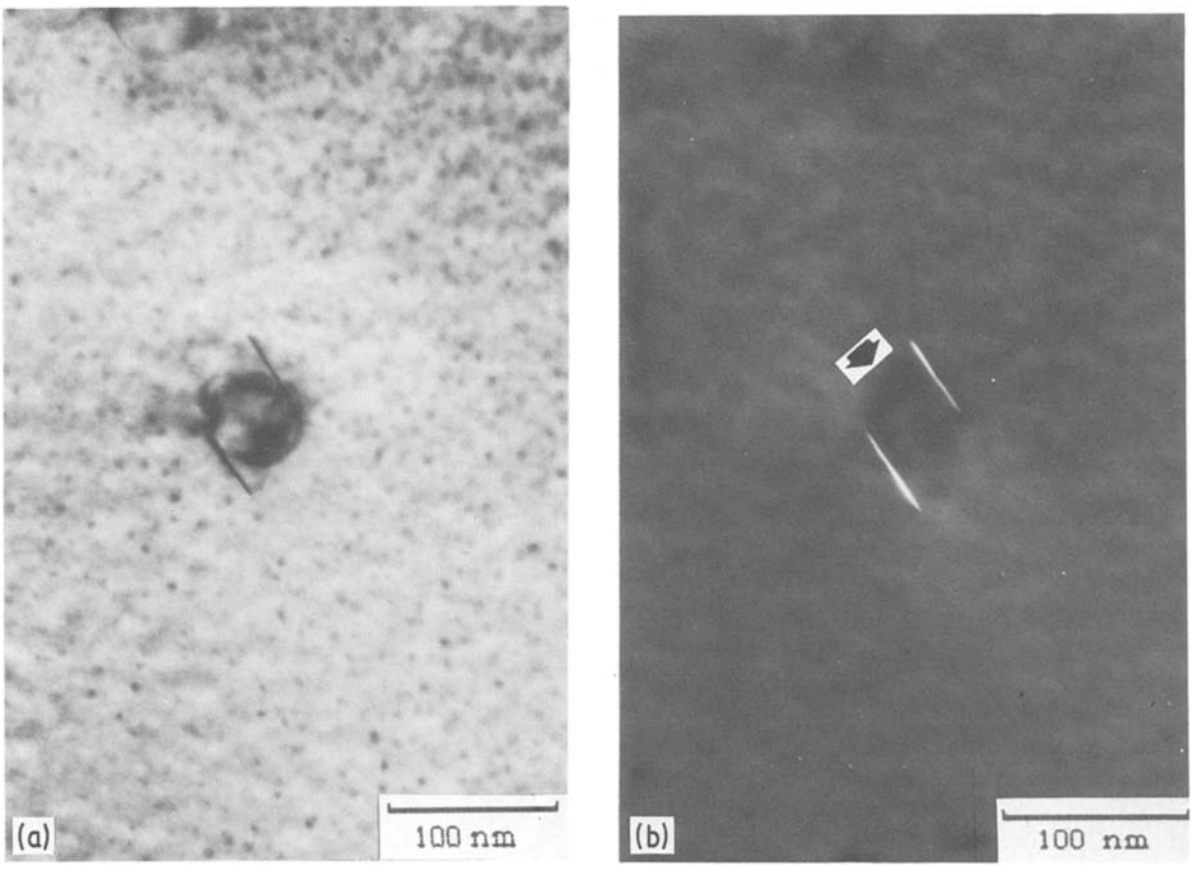

Figure 10 Nucleation of T_1 on the β'/matrix interface; (a) bright field image. The mottled contrast in the matrix is due to a very fine dispersion of δ'; (b) corresponding T_1 dark field image.

solid–solid nucleation theory. In the following discussion, the nucleation of the broad, coherent face of θ' on β' will be treated specifically while T_1 heterogeneous nucleation on β' can be described in a similar manner.

The occurrence of a specific lattice orientation relationship between θ' precipitates and the aluminium matrix allows the development of planar facets parallel to the optimally matching $(0\,0\,1)_\alpha$/$(0\,0\,1)_{\theta'}$ interfaces. Thus, the critical nucleus of θ' is likely to be faceted, and these facets will be parallel to the $\{1\,0\,0\}$ planes and of the energy cusp type [14].

Considering homogeneous nucleation first, Gibbs [13] has shown that when the precipitate/matrix boundary is independent of orientation the shape of the critical nucleus is a sphere of radius r^*. The energy barrier to nucleation (ΔG^*) is then given by

$$\Delta G^*_{hu} = (16\gamma^3_{\alpha/\beta}\pi)/(3\Delta G^2_v) \quad (1)$$

where $\gamma_{\alpha/\beta}$ is the specific interfacial free energy of the critical nucleus, ΔG_v is the volume free energy change, and the subscripts "h" and "u" designate "homogeneous" and "unfaceted". Johnson *et al.* [14] have shown that if an energy cusp appears at a specific boundary orientation of a homogeneously formed nucleus, ΔG^* is given by

$$\Delta G^* = \Delta G^*_{hu}[1 - 2f(\phi)] \quad (2)$$

where $f(\phi)$ is defined as

$$f(\phi) = (2 - 3\cos\phi + \cos^3\phi)/4 \quad (3)$$

and ϕ is the angle between the facet plane and the spherical boundary tangent at the point where the facet truncates the sphere (see Fig. 11). In addition, Gibbs [13] has shown that the ratio $\Delta G^*/\Delta G^*_{hu}$ is equal to the ratio of the volumes of the two different critical nuclei whose morphologies are based upon the sphere.

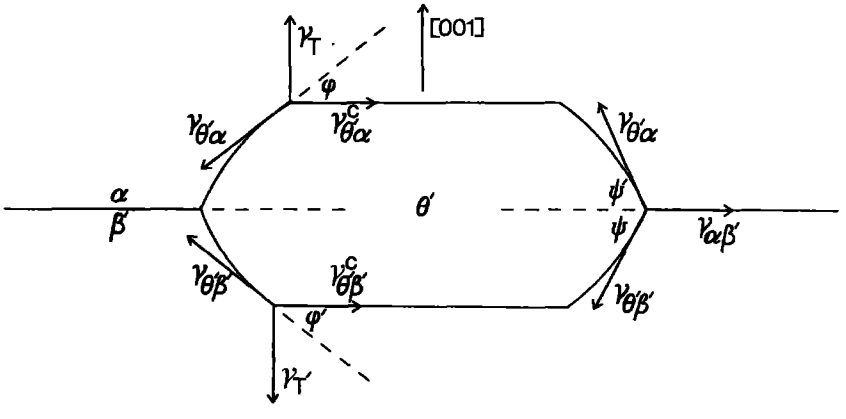

Figure 11 A schematic drawing of an equilibrium θ' nucleus on a β'/matrix interface. The various interfacial energy terms are: γ_T is the torque term associated with the θ'/α facet, $\gamma^c_{\theta'/\alpha}$ is the energy of the θ'/α facet, $\gamma_{\theta'/\alpha}$ is the energy of the curved θ'/α interface, $\gamma_{\theta'/\beta'}$ is the energy of the curved θ'/β' interface, $\gamma_{T'}$ is the torque term associated with the θ'/β' facet, $\gamma^c_{\theta'/\beta'}$ is the energy of the θ'/β' facet, and $\gamma_{\alpha/\beta'}$ is the energy of the α/β' interface.

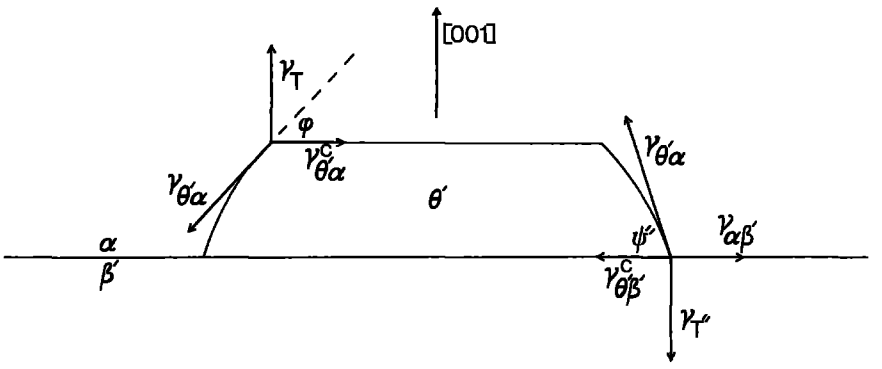

Figure 12 A schematic illustration of a "quasi-equilibrium" θ' nucleus. γ_T is the torque term associated with the $\alpha/\beta'/\theta'$ triple junction.

Since faceting can markedly reduce the volume of the critical nucleus, it can appreciably decrease ΔG^* [14]. Although the other variables in the general equation for the rate of nucleation are altered by faceting, it has been shown that the major influence of faceting upon nucleation kinetics is through its ability to decrease ΔG^* [14, 15].

Finally, consider the nucleation of a third phase, θ', at the interface between α and β'. Since the matrix and β' differ in composition but have the same crystal structure and identical lattice orientations, it can be postulated that facets will appear in both the matrix and β' precipitate. The two facets will be parallel, but, in general, will truncate different portions of the spheres of radii r and r'. The hypothetical arrangement is shown in Fig. 11. For simplicity, the radius of the β' has been taken to be much greater than that of the critical nucleus so that the α/β' interface is effectively planar. In addition, the energies of the interfaces in the $[0\,0\,1]_\alpha/[0\,0\,1]_{\theta'}$ zone are taken to be constant: i.e. no subsidiary minima occur in the Wulff plot. The two spherical boundaries of the θ' nucleus are of different radii r and r' since the energies between the θ' nucleus and the matrix and β' grains, $\gamma_{\theta'/\alpha}$ and $\gamma_{\theta'/\beta'}$, are likely to be different. In order to assure that the chemical potential of both disordered boundaries are equal

$$r^* = -(2\gamma_{\theta'/\alpha})/\Delta G_v \tag{4}$$

and

$$r'^* = -(2\gamma_{\theta'/\beta'})/\Delta G_v \tag{5}$$

Substituting these values into the equation for free energy of formation yields

$$\Delta G^* = \Delta G^*_{hu}\{[f(\psi) - f(\phi')] + (\sin^3\psi/\sin^3\psi')[f(\psi') - f(\phi)]\} \tag{6}$$

The final form of this equation suggests that this θ' nucleus morphology provides two mechanisms for the reduction of ΔG^*: (a) the destruction of the β'/matrix interface; and (b) the occurrence of planar facets.

The combined effects of these two mechanisms can result in a significant reduction in ΔG^* [14].

Experimentally, however, it was found in this investigation that the θ' plate-shaped precipitates have facets which extend into the matrix but do not penetrate into the β' precipitates, at least not to any appreciable extent that can be resolved (see Figs 3 to 10). This suggests that the θ' critical nucleus does not take the form of the predicted equilibrium shape. This observation may be explained by the very low diffusion kinetics of zirconium at the ageing temperature of 190° C. In order for the θ' nucleus to obtain an equilibrium shape, copper must diffuse into the β' while zirconium diffuses out of the β', but, at 190° C, the diffusivity of zirconium is very low. This "metastable" θ' nucleus morphology, however, results in an unbalance of the interfacial energy terms. The schematic arrangement for this observed precipitate shape is illustrated in Fig. 12. The energy barrier for critical nucleus formation in this situation is

$$\Delta G^* = \Delta G^*_{hu}[f(\psi'') - f(\phi)] \tag{7}$$

where the angles ψ'' and ϕ are given by

$$\cos\psi'' = (\gamma_{\alpha/\beta'} - \gamma^c_{\theta'/\beta'})/\gamma_{\theta'/\alpha} \tag{8}$$

and

$$\cos\phi = \gamma^c_{\theta'/\alpha}/\gamma_{\theta'/\alpha} \tag{9}$$

The ratio $\gamma^c_{\theta'/\alpha}/\gamma_{\theta'/\alpha}$, the energy of the coherent to the semi-coherent interface, has been determined to be 1 : 12 for θ' in binary Al–Cu [28, 29]. Thus, ϕ is approximately 85°. In the absence of data concerning $\gamma_{\alpha/\beta'}$ and $\gamma^c_{\theta'/\beta'}$, a value for ψ'' cannot be obtained. However, as long as $\psi'' \leqslant 180°$, or

$$\gamma^c_{\theta'/\beta'} \leqslant \gamma_{\alpha/\beta'} + \gamma_{\theta'/\alpha} \tag{10}$$

heterogeneous nucleation will be promoted. This inequality is likely to be satisfied since the θ'/β' interface is most probably coherent while the curved θ'/α interface will be semi-coherent.

Up to this point in the discussion, the influence of volume strain energy on ΔG^* has not been considered. The general expression for the free energy change associated with nucleation in the solid state is

$$\Delta G^0 = V(\Delta G_v + \Delta G_s) + A\gamma \tag{11}$$

The two terms representing the barrier to nucleation are the misfit strain energy, ΔG_s, per unit volume and the interfacial free energy, γ, per unit area, (V is the volume, and A is the area of the nucleus). In the discussion above, the interfacial free energy term alone was considered.

The metastable θ' phase has a relatively low surface energy but a high elastic strain energy. Therefore, it will tend to nucleate on dislocations where it can lower its strain energy. Since θ' nucleates on dislocations, room temperature deformation after

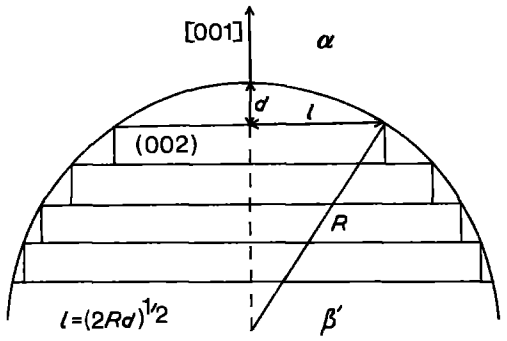

Figure 13 A representation of the terrace/ledge structure of a spherical β' precipitate. For discussion, see text.

solution heat treatment and prior to ageing increases the nucleation rate of this phase. In addition, interfacial dislocations surrounding β' could be generated by this deformation thereby creating preferential nucleation sites.

Some discussion is necessary for the occurrence of the semi-coherent edge of θ' plates being in contact with β'. This situation was observed predominantly in the 2% Li–3% Cu alloy. It is not likely that the above discussion concerning interfacial energy arguments can be applied to this case. It is postulated that one or both of the following explanations apply: (a) θ' nucleates on an interfacial dislocation surrounding the β' and/or (b) θ' impinges onto β' during growth.

Finally, the assumption that the α/β' interface is effectively planar requires consideration since the exact nature of the α/β' interface will determine the structure and energy of both the θ'/β' and T_1/β' interfaces. That the assumption is generally valid can be shown as follows for the case of θ' nucleating on β'. Consider a spherical β' precipitate of radius R. In the region where the local interface normal is [0 0 1], the surface of the β' can be considered in terms of a terrace/ledge structure; the terraces being parallel to (0 0 1) (Fig. 13). If the macroscopic α/β' interface is perfectly spherical, then the maximum radius of the first terrace, l, is given by:

$$R^2 = (R - d)^2 + l^2 \qquad (12)$$

where d is the interplanar spacing of the (0 0 2) planes. Expanding and rearranging yields

$$l^2 = 2Rd - d^2 \qquad (13)$$

Since $2Rd \gg d^2$

$$l = (2Rd)^{1/2} \qquad (14)$$

Using $d = 0.202\,\text{nm}$ and a typical value for R of 20 nm yields $l \cong 2.8\,\text{nm}$ which is likely to be comparable to the size of a critical nucleus. For example, Baumann and Williams [30] have shown that for an Al–7.9 at % Li binary alloy the critical δ' radius at a temperature approximately 50° C below the δ' solvus is 2 nm. Hence, the assumption of a planar α/β' interface is justified.

5. Summary

The major findings of this investigation can be summarized as follows:

1. Both θ' and, to a lesser extent, T_1 can nucleate at the β' $(Al_3Zr)/\alpha$–matrix interface.
2. In the vast majority of cases, the broad face of the θ' and/or T_1 is in contact with the β'.
3. Nucleation of the plate-like phases on the β'/α interface can be rationalized in terms of classical nucleation theory.
4. In the case where the semi-coherent edge of the plate-shaped precipitates is in contact with the β', no unambiguous evidence for the nucleation of θ' or T_1 has been obtained.

Acknowledgements

One of the authors (M. H. T.) gratefully acknowledges the Alloy Technology Division of Alcoa Laboratories, Alcoa Center, PA for financial support in the form of a Grant-in-Aid. Valuable discussions with Dr A. K. Vasudévan are also acknowledged.

References

1. T. H. SANDERS Jr and E. A. STARKE Jr, (eds) in "Aluminum-Lithium Alloys" (TMS-AIME, Warrendale, PA. 1981).
2. T. H. SANDERS Jr and E. A. STARKE Jr, (eds) in "Aluminum-Lithium Alloys II" (TMS-AIME, Warrendale, PA, 1984).
3. A. K. VASUDEVAN, R. C. MALCOM, W. G. FRICKE and R. J. RIOJA, "Resistance to Fracture, Fatigue and Stress of Al–Cu–Li–Zr Alloys", Final Report, NAVAIR Contract No. N00019-80-C-0569, (1985).
4. E. NESS and N. RYUM, *Scripta. Metall.* **5** (1971) 987.
5. E. NESS, *Acta Metall.* **20** (1972) 499.
6. W. STIMSON, M. H. TOSTEN, P. R. HOWELL and D. B. WILLIAMS, in Proceedings of the 3rd International Al–Li Conference, Oxford (The Institute of Metals, London, 1986).
7. P. L. MAKIN and B. RALPH, *J. Mater. Sci.* **19** (1984) 3835.
8. P. J. GREGSON and H. M. FLOWER, *J. Mater. Sci. Lett.* **3** (1984) 829.
9. M. H. TOSTEN, A. K. VASUDEVAN and P. R. HOWELL, in Proceedings of the 3rd International Al–Li Conference, Oxford (The Institute of Metals, London, 1986) p. 490.
10. R. F. HEHEMANN, in "Phase Transformations" (ASM, Metals Park, Ohio, 1970) p. 397.
11. C. W. SPENCER and D. J. MACK, in "Decomposition of Austenite by Diffusional Processes" (Interscience, New York, 1962) p. 549.
12. R. B. NICHOLSON, in "Phase Transformations" (ASM, Metals Park, Ohio, 1970) p. 269.
13. J. W. GIBBS, in "On the Equilibrium of Heterogeneous Substances, Collected Works" (Longsmans, New York, 1928).
14. W. C. JOHNSON, C. L. WHITE, P. E. MARTH, P. K. RUF, S. M. TUOMINEN, K. D. WADE, K. C. RUSSELL and H. I. AARONSON, *Metall. Trans. A* **6A** (1975) 911.
15. P. E. MARTH, H. I. AARONSON, G. W. LORIMER, T. L. BARTEL and K. C. RUSSELL, *Metall. Trans. A* **7A** (1976) 1519.
16. J. M. SIMERSKA and V. SYNECEK, *Acta. Metall.* **15** (1967) 223.
17. M. H. JACOBS and D. W. PASHLEY, in "The Mechanism of Phase Transformations in Crystalline Solids" (Institute of Metals, London, 1969) p. 43.
18. G. W. LORIMER, *Fizika* **2** (1970) 331.
19. G. W. LORIMER and R. B. NICHOLSON, in "The Mechanism of Phase Transformations in Crystalline Solids" (Institute of Metals, London, 1969) p. 36.
20. G. W. LORIMER and R. B. NICHOLSON, *Acta. Metall.* **14** (1966) 1009.

21. P. N. T. UNWIN, G. W. LORIMER and R. B. NICHOLSON, *ibid.* **17** (1969) 136.
22. H. A. HOLL, *Metal Sci. J.* **1** (1967) 111.
23. D. W. PASHLEY, J. RHODES and A. DENDOREK, *J. Inst. Met.* **94** (1966) 41.
24. D. W. PASHLEY, M. H. JACOBS and J. T. VIETZ, *Phil. Mag.* **16** (1967) 51.
25. J. P. SIMON and P. GUYOT, *J. Mater. Sci.* **12** (1978) 202.
26. D. VAUGHAN, *Acta. Metall.* **16** (1968) 563.
27. B. FOREST and M. BISCONDI, *J. Mater. Sci.* **12** (1978) 202.
28. H. I. AARONSON, J. B. CLARK and C. LAIRD, *Met. Sci. J.* **2** (1968) 155.
29. R. D. DOHERTY, *Met. Sci.* **16** (1982) 1.
30. S. F. BAUMANN and D. B. WILLIAMS, *Scripta. Metall.* **18** (1984) 611.

Received 25 October
and accepted 20 December 1985